Applied Surface Science 414 (2017) 230–237

Contents lists available at ScienceDirect

Applied Surface Science

journal homepage: www.elsevier.com/locate/apsusc

Long-term antibacterial characteristics and cytocompatibility of titania nanotubes loaded with Au nanoparticles without photocatalytic effects

Guomin Wang[a], Hongqing Feng[a,b,*], Weihong Jin[a], Ang Gao[a], Xiang Peng[a], Wan Li[a], Hao Wu[a], Zhou Li[b], Paul K. Chu[a,**]

[a] Department of Physics and Materials Science, City University of Hong Kong, Tat Chee Avenue, Kowloon, Hong Kong, China
[b] Beijing Institute of Nanoenergy and Nanosystems, Chinese Academy of Sciences, National Center for Nanoscience and Technology (NCNST), Beijing 100083, PR China

ARTICLE INFO

Article history:
Received 21 December 2016
Received in revised form 30 March 2017
Accepted 7 April 2017

Keywords:
Long-term antibacterial properties
Au-loaded titania nanotubes
ROS-free
Cytocompatibility

ABSTRACT

Au nanoparticles (NPs) can endow titania nanotubes (Au@TiO_2-NT) with light-independent antibacterial properties which bode well for *in vivo* application because of the dark environment inside tissues. In this work, the long-term antibacterial bactericidal properties and cytocompatibility of Au@TiO_2-NT without photocatalytic effects are studied in details. The materials exhibit antibacterial effects against *Staphylococcus aureus* according to antibacterial tests carried out for a total time of 21 days, which are normally long enough for early stage tissue healing after surgery. In addition, adhesion and proliferation of MC3T3-E1 osteoblasts on Au@TiO_2-NT reveal cytocompatibility comparable to that of TiO_2-NT. No reactive oxygen species (ROS) are detected from either the bacteria or MC3T3-E1 cells cultured on the Au@TiO_2-NT surface. The absence of ROS, long-term antibacterial properties, and cytocompatibility make Au@TiO_2-NT promising biomaterials in orthopedic devices and implants.

1. Introduction

Titania nanotubes (TiO_2-NT) have promising applications in orthopedic devices and implants due to their nanoscale texture similar to the natural bone matrix and potential of drug delivery [1–4]. A nanostructured surface is also believed to meet the criteria for bionic materials because natural bones are composed of collagen fibers and hydroxyapatite on the nanoscale [5,6]. In spite of recent advances in TiO_2-NT research, pristine TiO_2 does not have the antibacterial ability unless catalyzed by ultraviolet light (UV) [7–11]. Nevertheless, light cannot penetrate tissues to reach implants inside the body and there have been efforts to improve the bactericidal activity of TiO_2 with less dependence on UV [12–18]. In this respect, Ag-TiO_2 or Ag_2O-TiO_2 materials have bactericidal effects in the absence of light due to the direct effect of Ag NPs or release of Ag^+ [19–22]. Recently, Li et al. found that TiO_2-NT modified with Au nanoparticles (Au NPs) could inactivate bacteria efficiently in the absence of light [23]. In addition, our previous work suggested that Au@TiO_2-NT inhibited *Staphylococcus aureus* in the absence of light *via* an electron transfer based but reactive oxygen species (ROS) free process [24].

Although light-independent antibacterial effects of Au@TiO_2-NT have been observed, some issues are still not well understood or need improvement. For instance, the long-term antibacterial effects are required to combat bacterial infection while tissues heal [25–28]. Materials with good bacteria killing stability are usually considered to have long-term antibacterial properties [29] and biomaterials are typically assessed by reusing the materials to kill bacteria during storage for a certain period of time [20,21]. Hao et al. investigated the long-term antibacterial properties of decorated carbon nanotubes by carrying out experiments in 21 days [30]. Similarly, Ag@Fe_2O_3-GO nanocomposites were found to have long-term antibacterial characteristics after storage for 7 days [31]. However, there have been few studies on the evaluation of the long-term antibacterial properties of Au@TiO_2-NT. In addition, a light-independent bactericidal system causing no deleterious effects on cells is highly desirable and imperative to clinical

* Corresponding author at: Department of Physics and Materials Science, City University of Hong Kong, Tat Chee Avenue, Kowloon, Hong Kong, China. Beijing Institute of Nanoenergy and Nanosystems, Chinese Academy of Sciences, National Center for Nanoscience and Technology (NCNST), Beijing 100083, PR China.
** Corresponding author at: Department of Physics and Materials Science, City University of Hong Kong, Tat Chee Avenue, Kowloon, Hong Kong, China.
E-mail addresses: fenghongqing@binn.cas.cn (H. Feng), paul.chu@cityu.edu.hk (P.K. Chu).

http://dx.doi.org/10.1016/j.apsusc.2017.04.053
0169-4332/

adoption. Improved osseointegration has been observed from different nanostructures such as nanotubes, nanorods, nanogratings, and nanoflowers [32–36] but to the best of our knowledge, there have been few studies on the cytocompatibility and antibacterial mechanism of Au@TiO_2-NT as well. As molecules associated with the foreign body response [37], reactive oxygen species (ROS) are usually generated in tissue cells due to the presence of foreign biomaterials [38]. Although the intracellular ROS of *S. aureus* cannot be increased by Au@TiO_2-NT, this may not be true for tissue cells because mammalian cells and bacteria may respond differently in the same environment [39]. In this work, the long-term antibacterial properties and cytocompatibility of Au@TiO_2-NT are investigated. Bacterial inactivation is investigated every 7 days for a total 21 days by colony forming units (CFU) counting and scanning emission microscopy (SEM), and quantitative determination of intracellular superoxide verifies the ROS free antibacterial mechanism. The Au@TiO_2-NT also exhibits satisfactory cytocompatibility comparable to that of pristine TiO_2-NT without the generation of ROS.

2. Experimental details

2.1. Sample preparation and characterization

2.1.1. Sample preparation

Titanium foils (99.95% pure with a thickness of 0.14 mm) were cut into circles with a diameter of 12 mm and cleaned ultrasonically in acetone, alcohol, and deionized water sequentially for 5 min each. The specimens were taken out with a tweezer and dried in nitrogen. Afterwards, they were anodized in 100 mL of electrolyte (0.55 g of ammonium fluoride, 5 mL of methanol, 5 mL of deionized water, and 90 mL of ethylene glycol) for 1 h at 60 V supplied by a DC Source Meter (ITECT, America). After anodization, the specimens were immediately washed with deionized water and ultrasonically cleaned to remove the remaining electrolyte as well as undesired irregular oxide layer on the surface [21]. After drying in nitrogen, the specimens were mounted on a sample stage in a magnetron sputtering instrument equipped with a gold target and Au NPs were deposited on the surface for 10 s, 40 s, and 70 s at a sputtering current of 10 mA. The pressure in the vacuum chamber was 3×10^{-3} Pa. The distance between the gold target and sample was 60 mm and the sputtering rate was 20 nm/min. After deposition, the specimens were annealed at 450 °C for 3 h. Our experiments showed that the antibacterial rate and tissue cell proliferation on Ti and TiO_2-NT were similar to those on a petri dish (Fig. S1). Four groups of specimens were prepared for this study: TiO_2-NT (control), TiO_2-NT loaded by Au for 10 s, 40 s and 70 s (named 10 s Au@TiO_2-NT, 40 s Au@TiO_2-NT and 70 s Au@TiO_2-NT), respectively.

2.1.2. Sample characterization

The morphology of the samples with/without Au was observed by scanning electron microscopy (SEM, JSM 7001F, JEOL, Japan). The emission voltage and working distance were 5 kV and 10 mm, respectively. Energy-dispersive X-ray spectroscopy (EDS) was used to semi quantitatively determine the Au content near the surface and atomic force microscopy (AFM, Veeco MultimodeV) was employed to examine the surface morphology and roughness. X-ray diffraction (XRD, Siemens D500, Philips, Netherlands) with Cu Kα irradiation (λ = 1.54184 Å) was conducted to determine the crystallinity of samples at 30 kV and 10 mA. X-ray photoelectron spectroscopy (XPS, K-Alpha, Thermo Fisher Scientific, USA) with Al Kα radiation was used to determine the chemical states of the specimens with the peaks referenced to the C 1s peak at 284.6 eV. The XRD and XPS results were analyzed by MDI Jade 6.0 and XPS peak fitting, respectively and more details about the sample preparation details can be found from our previous study [24].

2.2. Effects on bacteria

2.2.1. Long-term antibacterial effect

Compared with Gram-negative bacteria, the thicker membrane of Gram-positive bacteria makes them more difficult to kill [40]. Thus, *Staphylococcus aureus* (*S. aureus*, ATCC29213) is again selected as the model bacteria in this study. A single colony of *S. aureus* was chosen and cultivated in Luria broth (LB) medium (10 g L^{-1} tryptone, 5 g L^{-1} yeast extract, 5 g L^{-1} NaCl) [41] on a rotatory shaker (220 rpm) overnight at 37 °C. The bacteria solution was diluted ten times with LB medium and cultivated at 37 °C for another 3 h to OD_{600} of 0.25–0.3 ($2–3 \times 10^9$ CFU mL^{-1}). The bacteria solution was diluted to a final concentration of $2–3 \times 10^5$ CFU mL^{-1} and 100 μL of the solution were spread on the sample surface. After 24 h, 900 μL of the medium were added and mixed with the remaining bacteria solution in each well. The bacteria solution was diluted to the proper concentration, spread on agar plates, and cultivated overnight at 37 °C. The CFUs were counted and analyzed. Afterwards, the specimens were ultrasonically cleaned, dried, sterilized, re-incubated as described above, and soaked in the simulated body fluid (SBF). After 6 days, the same antibacterial process was carried out on the samples used above and the inactivation rate was measured again for a cultivating time of 24 h. This process lasted for three weeks as described in the previous study [21].

2.2.2. Morphology of treated S. aureus

SEM was performed to examine the morphology of the bacteria after the treatment. After different treatment time durations, the samples with bacteria were rinsed with 1 mL of PBS, fixed with 2.5% glutaraldehyde overnight, and dehydrated with ethanol with concentrations of 10%, 30%, 50%, 70%, 90%, and 100% (v/v) sequentially. The samples were dried in vacuum at room temperature and mounted on the specimen stage and a 10 nm thick Au layer was sputter-deposited prior to observation.

2.2.3. Quantitative analysis of intracellular superoxide

The intracellular superoxide was determined quantitatively with a Superoxide Assay Kit (S0060, Beyotime, China) according to the manufacturer's protocol. The bacteria cultivated on the samples for 3 h and 6 h were rinsed with PBS and collected by centrifugation (3000 × *g*, 5 min). 200 μL of the superoxide detection reagent were added to each well on a 96-well plate in which 100 μL of the treated bacteria had been added. After culturing at 37 °C for 3 min, the absorbance at 450 nm and 600 nm was recorded and analyzed.

2.3. Cytocompatibility of MC3T3-E1 osteoblasts

2.3.1. Cell culture

MC3T3-E1 osteoblasts purchased from the cell bank of Chinese Academy of Sciences were used to study the cytocompatibility of the Au@TiO_2-NT. The cells were cultured in dulbecco's modified eagle medium (DMEM) containing 10% fetal bovine serum (FBS) on 90 mm petri dishes. The dishes were put in an incubator at 37 °C with 5% CO_2 as the humidifying air. The culture medium was replaced with fresh medium every other day. To evaluate cell adhesion and cytotoxicity, the cells in the logarithmic growth phase were harvested, centrifuged at 1,000 rpm for 5 min, and adjusted to a density of 2×10^4 cells mL^{-1} before 1 mL of cells were seeded on each disinfected sample on a 24-well plate.

2.3.2. Cell adhesion

To observe adhesion after 4 h and 24 h, the cells were rinsed with PBS twice, fixed with 4% paraformaldehyde, permeabilized

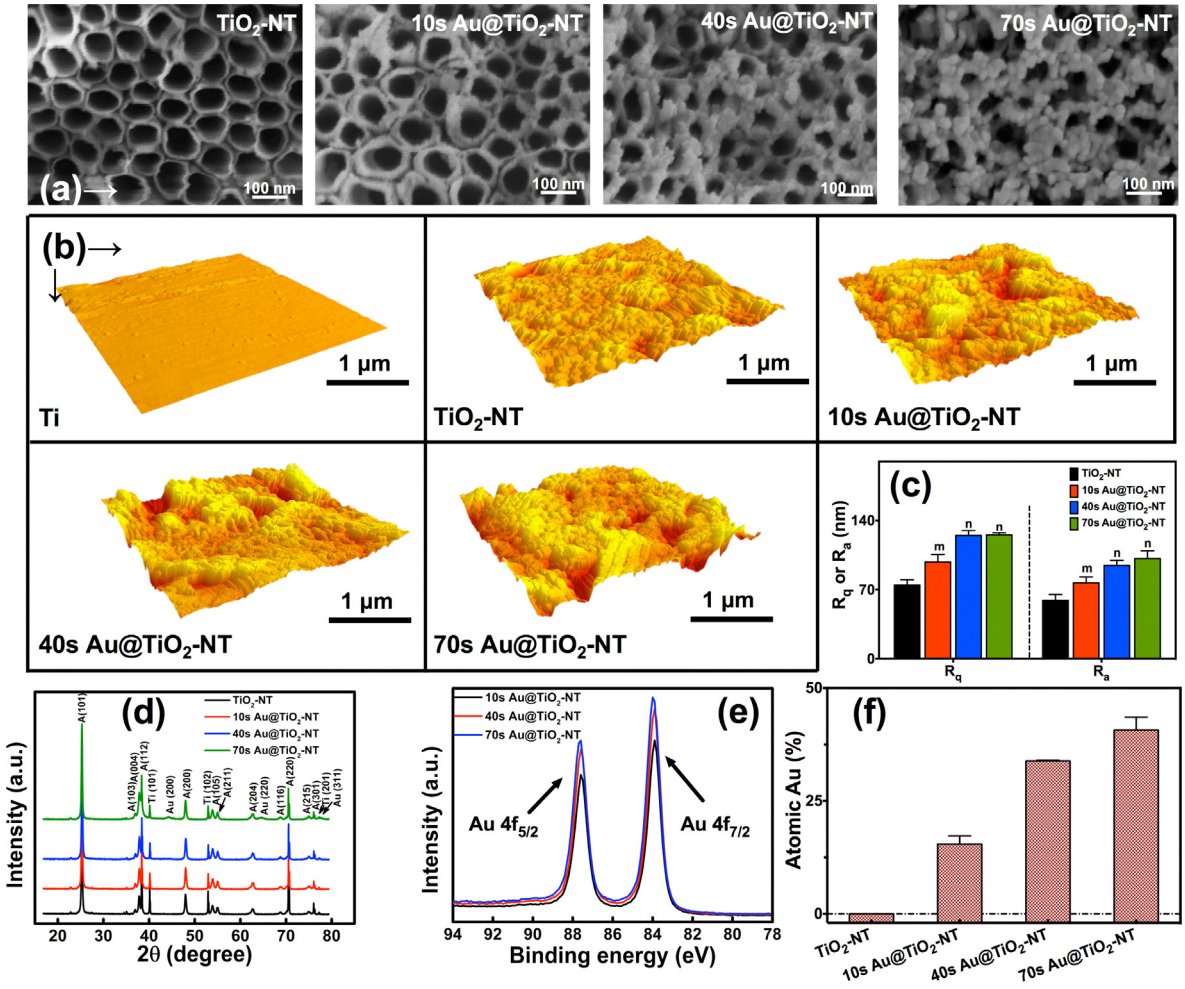

Fig. 1. SEM, AFM, XRD, XPS and EDS results: (a) surface morphology by SEM; (b) surface morphology by AFM; (c) surface roughness with significant difference between groups marked with different letters (m-n, $P < 0.05$); (d) XRD patterns with A meaning anatase TiO_2; (e) high-resolution XPS spectra of Au ($4f_{7/2}$ and $4f_{5/2}$) in Au@TiO_2-NT; (f) Au content determined by EDS.

with 0.2% Triton X-100 (sigma, USA), stained with phalloidin-fluorescein isothiocyanate (Sigma, USA) for 30 min, and stained with 4′, 6-diamidino-2-phenylindole (DAPI, sigma, USA) for 5 min. The samples were observed under an inverted microscope (20AYC, BM) at excitation/emission wavelengths of 358 nm/461 nm and 488 nm/520 nm, respectively.

2.3.3. Cell proliferation and viability

In this work, the 3-(4,5-dimethylthiazol-2-yl)-2,5-diphenyl tetrazolium bromide (MTT) test was carried out to evaluate cell proliferation and viability on the samples [21,42]. After culturing for 24 h, 72 h, and 120 h, the medium on the 24-well plate was replaced with the MTT solution and cultivated for 4 h. Afterwards, the MTT solution was replaced with dimethyl sulphoxide (DMSO) to dissolve the formazan crystals and 100 μL of the solution were transferred to a 96-well plate and measured by the Multimode Reader (BioTek, US) at the extinction wavelength of 570 nm. The wells with DMSO served as the negative control.

2.3.4. ROS detection in MC3T3-E1 osteoblasts

To determine the intracellular ROS level in the cells after treatment, the cells were cultivated on the samples on a 24-well plate. After treatment for 4 h and 24 h, the cells were rinsed with PBS twice and treated with 2′,7′-dichlorofluorescin diacetate (DCFH-DA) and DAPI for 30 min at 37 °C [43]. The samples with adhered cells were rinsed with PBS and examined under an inverted microscope at excitation/emission wavelengths of 358 nm/461 nm and 488 nm/520 nm, respectively. The cells stained blue represented cells adhering on the surface and green cells represent those with positive ROS signals.

2.4. Statistical analysis

The experiments were repeated at least 3 times. The results were presented as mean ± stand deviation (SD) and analyzed by the SNK test in ANOVA and Student's *t* test. A value of $P < 0.05$ was considered statistically significant.

3. Results and discussion

The characterization results are presented in Fig. 1. The morphology of the samples observed under SEM is depicted in Fig. 1a and fine NTs with an average diameter of ~100 nm are formed on the surface of the Ti plate. The size of the Au NPs increases gradually with time. After loading for 10 s, the Au NPs are about 10 nm in size. The size of the Au NPs in 40 s Au@TiO_2-NT and 70 s Au@TiO_2-NT is about 20 nm. The Au NPs are evenly distributed on the surface of the NTs after doping for 40 s but some Au NPs aggregate when the time is 70 s and they cover some of the nanotubes. AFM also reveals homogeneous nanotubes on the Ti surface after anodization for 1 h and Au NPs with different sizes are evenly distributed on the 10 s, 40 s and 70 s Au@TiO_2-NT samples. The morphology of

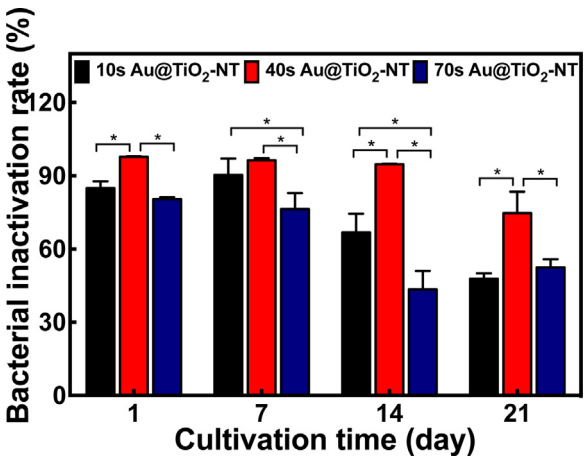

Fig. 2. Antibacterial assay of Au@TiO_2-NT for 21 days with significant differences marked as * ($P < 0.05$).

the TiO_2-NT becomes rougher after introduction of Au NPs (Fig. 1b) and the R_a and R_q values are shown in Fig. 1c. The roughness of 40 s Au@TiO_2 and 70 s Au@TiO_2-NT is larger than that of the other groups. A rougher surface with a larger surface area can enhance the interactions between biomaterials and bacteria [44–46].

Fig. 1d displays the XRD patterns of the samples with different Au loadings. The dominant diffraction peaks at $2\theta = 25.3^\circ$ (101), 48.0° (200), and 70.3° (220) observed from all the samples indicate formation of anatase TiO_2-NT which has better electrical activity than rutile and may also contribute to the easier electronic interaction between anatase TiO_2 and Au particles here [47,48]. The Ti (101), (102) and (201) phases are attributed to the limited microscale depth of TiO_2-NT. As the amount of loaded Au is relatively small and detection depth of XRD is relatively large, patterns corresponding to Au (200), (220) and (311) do not emerge until the TiO_2-NT is loaded with 70 s Au NPs. Nevertheless, the high-resolution Au ($4f_{7/2}$ and $4f_{5/2}$) XPS spectra with nanometer depth resolution indicate that the content of Au in the near surface of 40 s Au@TiO_2-NT is larger than that in 10 s Au@TiO_2-NT and smaller than that in 70 s Au@TiO_2-NT (Fig. 1e). The Au concentration increases from ~15% to ~40% with loading time from 10 s to 70 s (Fig. 1f). These results are in accordance with the atom concentrations of Ti, O, and Au determined by EDS in our previous work [24]. All in all, SEM, AFM, XRD, and XPS show evidence of the formation of Au@TiO_2-NT.

The antibacterial stability of materials, which is important in practical application, is usually affected by the storage time [49] which may also affect the long-term antibacterial stability of Au@TiO_2-NT [29]. Bacteria inactivation is conducted for three consecutive weeks to determine the long-term bactericidal effects of the Au@TiO_2-NT without light. After each antibacterial test, the samples are autoclaved and immersed in SBF until the next antibacterial test to mimic the *in vivo* environment. The results show that the antibacterial effect of 40 s Au@TiO_2-NT has a tendency to decrease with the antibacterial rate dropping from 99% in day 1 to 74% in day 21 (Fig. 2). The bacteria inactivation efficiency of 10 s Au@TiO_2-NT and 70 s Au@TiO_2-NT remains at ~90% during the first two bactericidal periods and decreases to ~50% during the two subsequent periods. The best long-term antibacterial effect is shown by 40 s Au@TiO_2-NT. As aforementioned, the rough surface on 40 s Au@TiO_2-NT may play an important role in the interaction between the bacteria and sample. Although the roughness of 40 s Au@TiO_2-NT and 70 s Au@TiO_2-NT is similar, they have different morphology (Fig. 1a), with the aggregating Au NPs in 70 s Au@TiO_2-NT hindering the bacteria-surface interaction. On the other hand, the antibacterial effect may also be determined by the suitable amount and size of Au NPs because size-dependent effects have been observed from NPs in other studies [50,51]. It is believed that the right distribution of Au NPs and surface roughness in 40 s Au@TiO_2-NT that result in the optimal electrical interaction between bacteria and sample surface leading to the best bactericidal effect. Our results disclose an optimal loading time for prevention of early, intermediate, and even late post-surgery infection [20].

SEM is performed to examine the morphology of *S. aureus* cultivated on different samples for 24 h. As TiO_2-NT without light cannot affect the growth of bacteria [9,52,53], TiO_2-NT is the control group. The amounts of adherent bacteria on 40 s Au@TiO_2-NT and ROS positive groups (0.1 mM H_2O_2 and TiO_2-NT + UV group) are much less than that on TiO_2-NT (Fig. 3), suggesting that neither 40 s Au@TiO_2-NT nor the ROS positive surface is favorable to bacteria growth. As for the morphology, the bacteria in TiO_2-NT group maintain a round normal shape while the remaining bacteria on 40 s Au@TiO_2-NT are connected and the shape of some single cells is deformed but little overflowing substances can be found (Fig. 3b). As the ROS positive control group, *S. aureus* treated with 0.1 mM H_2O_2 shows serious cytosolic content leakage and cell lysis (red arrows in Fig. 3c). The TiO_2-NT + UV group is similar with some of the cells suffering from severe damage (red arrows in Fig. 3d). Oxidative stress burst is suspected to undermine the membrane integrity causing overflow of intracellular substances [54]. The different bacteria responses to 40 s Au@TiO_2-NT and ROS positive groups suggest a different bacterial killing mechanism between 40 s Au@TiO_2-NT and the ROS dominated antibacterial process.

As essential signaling molecules, the ROS level reflects the living status of bacteria. Recent studies suggest that finding the exact role of intracellular ROS bodes well for practical approaches to enhance our current antibiotics arsenal [55–57]. Likewise, to better understand whether Au@TiO_2-NT induces ROS during the bacteria killing process can aid bone implant design and fabrication. Therefore, the

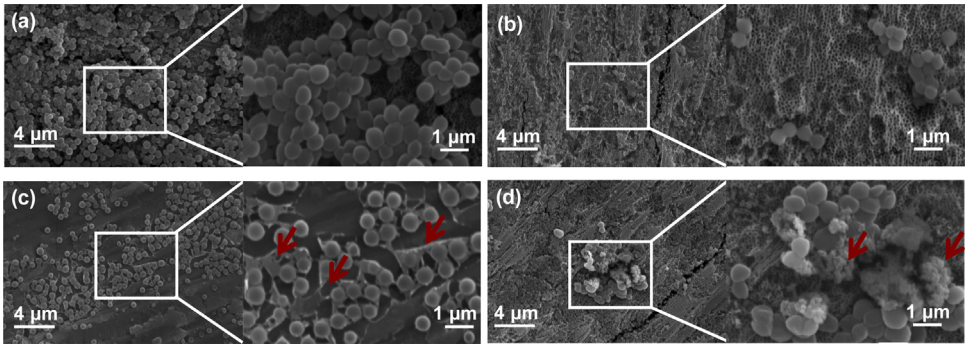

Fig. 3. Morphology of *S. aureus* cultured on the samples for 24 h under different conditions: (a) TiO_2-NT, (b) 40 s Au@TiO_2-NT, (c) Ti plate with 0.1 mM H_2O_2, and (d) TiO_2-NT irradiated with UV. (a)–(c) are in darkness. (For interpretation of the references to color in the text, the reader is referred to the web version of the article.)

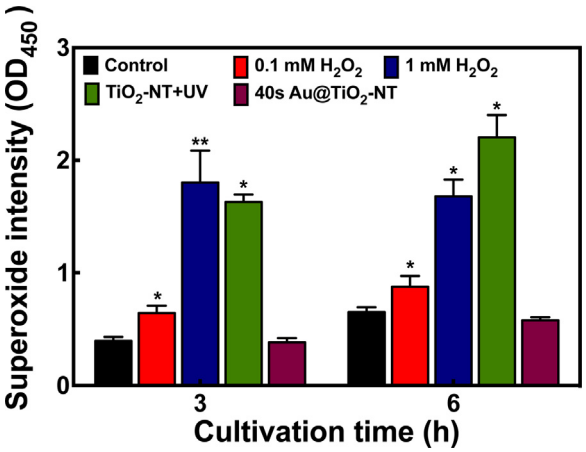

Fig. 4. Relative superoxide concentration in treated *S. aureus* with OD_{450} representing the intracellular superoxide level with * denoting $P < 0.05$ and ** denoting $P < 0.01$ compared to the control group.

generation of intracellular superoxide in each group is examined (Fig. 4). Superoxide is an important ROS that can destroy the activities of enzymes and integrity of DNA [58]. The superoxide levels increase when the H_2O_2 concentration increases and similarly, bacteria treated with TiO_2-NT + UV show a similar superoxide level as those treated with 1 mM H_2O_2. On the contrary, no superoxide is detected from the 40 s Au@TiO_2-NT group which shows the same level as the control group. Superoxide is considered vital in the ROS-dependent bacteria killing process [59]. Based on the significant difference between the H_2O_2 and TiO_2-NT + UV groups, the negative superoxide signal observed from the 40 s Au@TiO_2-NT group suggests an ROS-free interaction consistent with our previous results.

Titania is a suitable implant candidate material because of the inexpensiveness, good mechanical properties, and strong corrosion resistance [60]. Studies including ours (Fig. S1a) confirm that titania without light illumination is nontoxic to bacteria and is even better than pure titanium in supporting bacterial survival [9,24,52,53]. On the other hand, biomedical applications of Au NPs on genomics, biosensorics, immune assays and clinical chemistry have been widely investigated [61]. However, Au NPs have little antibacterial effects without modification or assistance from light [62,63]. Besides, the bacteria in the Au@Ti group grow similarly like those on Ti suggesting that Au NPs alone cannot kill bacteria either (Fig. S2). The previous data and results from this study verify the antibacterial effects of Au@TiO_2-NT that neither Au NPs nor TiO_2-NT alone can kill bacteria. Based on the bacteria-current between bacteria and Au@TiO_2-NT, electron light regions, slight bacteria membrane potential drop, as well as negative intracellular ROS signal detected from our previous study [24], it can be deduced that *S. aureus* die from electrons loss in an ROS-free process, which is again verified by the SEM bacteria morphology and the negative superoxide signal in this study.

In the assessment of cytocompatibility, the initial cell adhesion process is observed by fluorescent microscopy (Fig. 5). After culturing for 4 h, the cells in all the three Au@TiO_2-NT groups adhere to the samples similar to the TiO_2-NT control. Expression of filamentous F-actin in 40 s Au@TiO_2-NT is slightly less than that in other groups, but the intensity of the cells in the Au@TiO_2-NT groups increases in the following 20 h. After 24 h, the cells in the TiO_2-NT and Au@TiO_2-NT groups spread well showing similar filamentous F-actin amounts and distribution. Formation of F-actin observed from the Au@TiO_2-NT groups suggests that the Au@TiO_2-NT sustains suitable growth conditions for initial growth of tissue cells because F-actin is a cytoskeleton protein that plays important role in maintaining the cellular and tissue structure [64].

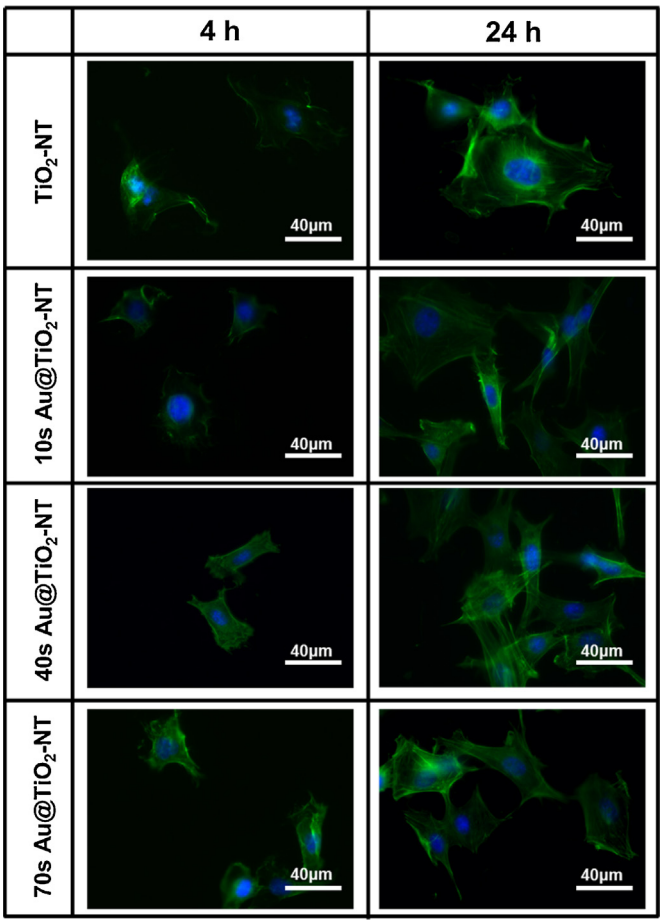

Fig. 5. Fluorescent images of MC3T3-E1 osteoblasts cultivated on different samples for 4 h and 24 h with actin stained as green and nuclei stained as blue. (For interpretation of the references to color in this figure legend, the reader is referred to the web version of the article.)

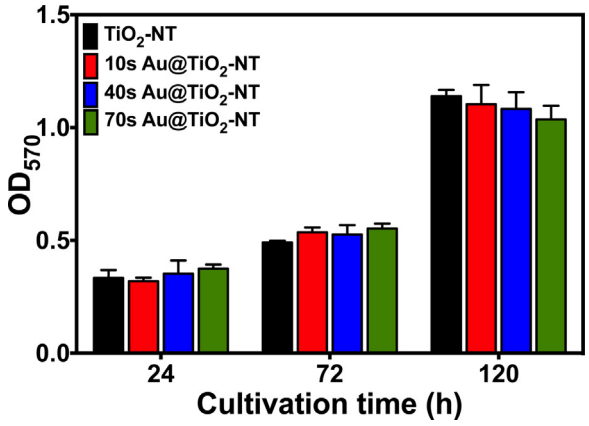

Fig 6. Time-dependent viabilities of MC3T3-E1 osteoblasts after culturing for 24, 72, and 120 h on the TiO_2-NT and Au@TiO_2-NT samples.

To quantitatively evaluate the long-term cytocompatibility, cell proliferation is monitored for 120 h. Similar to cell adhesion (Fig. 6), cell proliferation on the Au@TiO_2-NT groups show little difference from that in the TiO_2-NT group ($P > 0.05$). OD_{570} is about 0.3 after cultivating for 24 h, increases to about 0.5 in the following 48 h, and is about 1.1 after 120 h. The cell adhesion and viability data corroborate the slight negative impact on cytocompatibility by the Au@TiO_2-NT.

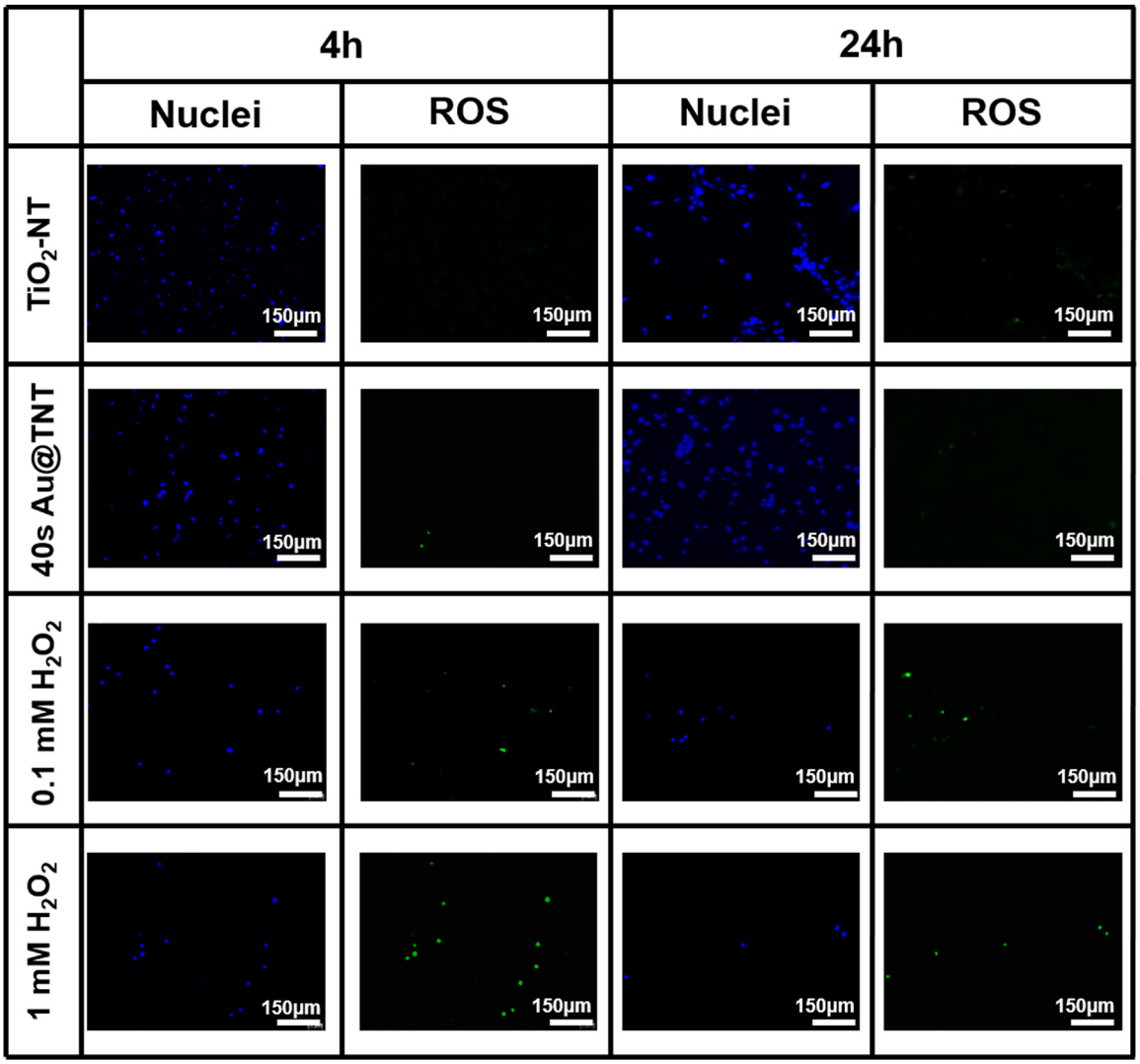

Fig. 7. Fluorescent images of MC3T3-E1 osteoblasts cultivated on different specimens for 4 h and 24 h stained with DCFH-DA (ROS) and DAPI (nuclei).

The intracellular ROS levels of the MC3T3-E1 cells are monitored by DCFH-DA staining assisted by simultaneous DAPI staining to show the cell numbers (Fig. 7). The amounts of nuclei on the TiO_2-NT and 40 s Au@TiO_2-NT groups are similar, but no ROS is observed from both groups. As the ROS positive groups, the nucleus densities in 0.1 mM H_2O_2 and 1 mM H_2O_2 are less than those in the other groups and most of the cells in the H_2O_2 groups are stained green by the ROS detector. The results demonstrate that the Au@TiO_2-NT does not alter the ROS levels of the MC3T3-E1 osteoblasts furnishing proof that no significant ROS-related oxidative stress is caused by the Au@TiO_2-NT to both bacteria and tissue cells in contrary to the photocatalytic mechanism of TiO_2 [65]. Besides, as the concentration of Au is even less than one third of the detection limit, little Au is leached into the solution (Fig. S3). Thus, the side effect by Au leaching can be excluded, highlighting the advantage of Au@TiO_2-NT over Ag-incorporated materials, in which Ag-leaching can cause tissue damage [7].

The similar nanoscale texture TiO_2-NT bodes well for its promising applications in orthopedic devices and implants. Although the photocatalytic antibacterial properties of TiO_2-NT have been studied, clinical application of TiO_2-NT as implants requires a light-independent antibacterial ability. We have observed light-independent antibacterial properties of Au@TiO_2-NT induced by extracellular electron transfer (EET) from the bacteria to the substrate [24]. That study focuses on the comparison between our bacteria-current and localized surface plasmon resonance (LSPR) as well as microbial fuel cells (MFC). In this work, we focus on whether the Au@TiO_2-NT substrate can maintain long-lasting antibacterial properties, has satisfactory cytocompatibility, and can induce ROS production in tissues. These issues must be understood before practical application. This work verifies the long-lasting antibacterial effects of Au@TiO_2-NT as well the antibacterial effect and the ROS-free antibacterial mechanism thereby supplying essential information enabling more expeditious clinical adoption.

Biomaterials with intrinsic compatibility and antibacterial characteristics are highly desirable in clinical applications. Although antibacterial surfaces have been widely studied, simultaneous antibacterial properties and biocompatibility are still challenging. In this work, Au@TiO_2-NT interacts with bacteria, causes steady electrons loss, and finally leads to bacteria death during the 24 h antibacterial process, which can be recycled four times in 21 days. Previous studies focusing on the drug-delivery property of TiO_2-NT have also shown long-term antibacterial effects by antibiotics or antimicrobial peptides immobilization on the TiO_2-NT [66,67]. In the future, the inorganic antibacterial system described here can be combined with antibiotics or antibacterial peptides to achieve even better antibacterial effects. The combination of Au@TiO_2-NT with antibiotics may reduce the amount of antibiotics required, facilitate

attachment of antibiotics, and help to disinfect the drug-resistant bacteria.

The Au@TiO_2-NT does not induce intracellular ROS in the bacteria or osteoblasts and this process is different from the common ROS-related antibacterial process [68,69], which is prone to causing cell damage or even cancer [70]. Favorable cytocompatibility is observed from the Au@TiO_2-NT as reflected by good adhesion and growth of osteoblasts. Since the nanotubes mimic the surface nanotopography of bones and the Au NPs do not introduce deleterious effects to osteoblasts, good cytocompatibility is accomplished [71]. The different responses between bacteria and osteoblasts may be ascribed to the different size and structure [72] and the overall results in this study suggest the large potential of Au@TiO_2-NT in orthopedic applications.

4. Conclusion

Au@TiO_2-NT with the desirable nanotopography shows long-term antibacterial characteristics against *S. aureus* without photocatalytic effects. The negative intracellular superoxide signal in *S. aureus* treated with the Au@TiO_2-NT confirms an ROS-free antibacterial mechanism. The good cytocompatibility results suggest that the Au@TiO_2-NT sustains a favorable environment for osteoblasts without intracellular ROS and this study provides evidence about the feasibility of Au@TiO_2-NT as light-independent bactericidal materials for clinical applications.

Conflict of interest

The authors declare no competing financial interests.

Acknowledgements

This work was financially supported by Hong Kong Research Grants Council (RGC) General Research Funds (GRF) No. CityU 11301215 and National Natural Science Foundation of China (NSFC) 81601629.

Appendix A. Supplementary data

Supplementary data associated with this article can be found, in the online version, at http://dx.doi.org/10.1016/j.apsusc.2017.04.053.

References

[1] X. Chen, A. Selloni, Introduction: titanium dioxide (TiO_2) nanomaterials, Chem. Rev. 114 (2014) 9281–9282.
[2] K. Lee, A. Mazare, P. Schmuki, One-dimensional titanium dioxide nanomaterials: nanotubes, Chem. Rev. 114 (2014) 9385–9454.
[3] Z. Wang, C. Xie, F. Luo, P. Li, X. Xiao, P25 nanoparticles decorated on titania nanotubes arrays as effective drug delivery system for ibuprofen, Appl. Surf. Sci. 324 (2015) 621–626.
[4] Y. Parcharoen, P. Kajitvichyanukul, S. Sirivisoot, P. Termsuksawad, Hydroxyapatite electrodeposition on anodized titanium nanotubes for orthopedic applications, Appl. Surf. Sci. 311 (2014) 54–61.
[5] G. Wang, J. Li, K. Lv, W. Zhang, X. Ding, G. Yang, X. Liu, X. Jiang, Surface thermal oxidation on titanium implants to enhance osteogenic activity and *in vivo* osseointegration, Sci. Rep. 6 (2016), 31769.
[6] R. Murugan, S. Ramakrishna, *In situ* formation of recombinant humanlike collagen-hydroxyapatite nanohybrid through bionic approach, Appl. Phys. Lett. 88 (2006) 193124.
[7] S. Eckhardt, P.S. Brunetto, J. Gagnon, M. Priebe, B. Giese, K.M. Fromm, Nanobio silver: its interactions with peptides and bacteria, and its uses in medicine, Chem. Rev. 113 (2013) 4708–4754.
[8] C.A. Linkous, G.J. Carter, D.B. Locuson, A.J. Ouellette, D.K. Slattery, L.A. Smitha, Photocatalytic inhibition of algae growth using TiO_2, WO_3, and cocatalyst modifications, Environ. Sci. Technol. 34 (2000) 4754–4758.
[9] Y. Kikuchi, K. Sunada, T. Iyoda, K. Hashimoto, A. Fujishima, Photocatalytic bactericidal effect of TiO_2 thin films: dynamic view of the active oxygen species responsible for the effect, J. Photochem. Photobiol. A 106 (1997) 51–56.
[10] D.J. Novo, N.G. Perlmutter, R.H. Hunt, H.M. Shapiro, Multiparameter flow cytometric analysis of antibiotic effects on membrane potential, membrane permeability, and bacterial counts of *Staphylococcus aureus* and *Micrococcus luteus*, Antimicrob. Agents Chemother. 44 (2000) 827–834.
[11] H. Cai, X. Chen, Q. Li, B. He, Q. Tang, Enhanced photocatalytic activity from Gd, La codoped TiO_2 nanotube array photocatalysts under visible-light irradiation, Appl. Surf. Sci. 284 (2013) 837–842.
[12] C. Hu, Y. Lan, J. Qu, X. Hu, A. Wang, Ag/AgBr/TiO_2 visible light photocatalyst for destruction of azodyes and bacteria, J. Phys. Chem. B 110 (2006) 4066–4072.
[13] M.-S. Wong, W.-C. Chu, D.-S. Sun, H.-S. Huang, J.-H. Chen, P.-J. Tsai, N.-T. Lin, M.-S. Yu, S.-F. Hsu, S.-L. Wang, Visible-light-induced bactericidal activity of a nitrogen-doped titanium photocatalyst against human pathogens, Appl. Environ. Microbiol. 72 (2006) 6111–6116.
[14] T.-S. Wu, K.-X. Wang, G.-D. Li, S.-Y. Sun, J. Sun, J.-S. Chen, Montmorillonite-supported Ag/TiO_2 nanoparticles: an efficient visible-light bacteria photodegradation material, ACS Appl. Mater. Interfaces 2 (2010) 544–550.
[15] C. Karunakaran, G. Abiramasundari, P. Gomathisankar, G. Manikandan, V. Anandi, Cu-doped TiO_2 nanoparticles for photocatalytic disinfection of bacteria under visible light, J. Colloid Interface Sci. 352 (2010) 68–74.
[16] D.B. Hamal, J.A. Haggstrom, G.L. Marchin, M.A. Ikenberry, K. Hohn, K.J. Klabunde, A multifunctional biocide/sporocide and photocatalyst based on titanium dioxide (TiO_2) codoped with silver, carbon, and sulfur, Langmuir 26 (2009) 2805–2810.
[17] P. Wu, R. Xie, K. Imlay, J.K. Shang, Visible-light-induced bactericidal activity of titanium dioxide codoped with nitrogen and silver, Environ. Sci. Technol. 44 (2010) 6992–6997.
[18] S. Cao, B. Liu, L. Fan, Z. Yue, B. Liu, B. Cao, Highly antibacterial activity of N-doped TiO_2 thin films coated on stainless steel brackets under visible light irradiation, Appl. Surf. Sci. 309 (2014) 119–127.
[19] M. Li, M.E. Noriega-Trevino, N. Nino-Martinez, C. Marambio-Jones, J. Wang, R. Damoiseaux, F. Ruiz, E.M. Hoek, Synergistic bactericidal activity of Ag-TiO_2 nanoparticles in both light and dark conditions, Environ. Sci. Technol. 45 (2011) 8989–8995.
[20] L. Zhao, H. Wang, K. Huo, L. Cui, W. Zhang, H. Ni, Y. Zhang, Z. Wu, P.K. Chu, Antibacterial nano-structured titania coating incorporated with silver nanoparticles, Biomaterials 32 (2011) 5706–5716.
[21] A. Gao, R. Hang, X. Huang, L. Zhao, X. Zhang, L. Wang, B. Tang, S. Ma, P.K. Chu, The effects of titania nanotubes with embedded silver oxide nanoparticles on bacteria and osteoblasts, Biomaterials 35 (2014) 4223–4235.
[22] Q. Cheng, C. Li, V. Pavlinek, P. Saha, H. Wang, Surface-modified antibacterial TiO_2/Ag^+ nanoparticles: preparation and properties, Appl. Surf. Sci. 252 (2006) 4154–4160.
[23] J. Li, H. Zhou, S. Qian, Z. Liu, J. Feng, P. Jin, X. Liu, Plasmonic gold nanoparticles modified titania nanotubes for antibacterial application, Appl. Phys. Lett. 104 (2014) 261110.
[24] G. Wang, H. Feng, A. Gao, Q. Hao, W. Jin, X. Peng, W. Li, G. Wu, P.K. Chu, Extracellular electron transfer from aerobic bacteria to Au loaded TiO_2 semiconductor without light: a new bacteria killing mechanism other than localized surface plasmon resonance or microbial fuel cells, ACS Appl. Mater. Interfaces 8 (2016) 24509–24516.
[25] X. Bai, K. More, C.M. Rouleau, A. Rabiei, Functionally graded hydroxyapatite coatings doped with antibacterial components, Acta Biomater. 6 (2010) 2264–2273.
[26] M. Ma, M. Kazemzadeh-Narbat, Y. Hui, S. Lu, C. Ding, D.D. Chen, R.E. Hancock, R. Wang, Local delivery of antimicrobial peptides using self-organized TiO_2 nanotube arrays for peri-implant infections, J. Biomed. Mater. Res. A 100 (2012) 278–285.
[27] Y. Zhang, C. Hou, S. Yu, J. Xiao, Z. Zhang, Q. Zhai, J. Chen, Z. Li, X. Zhang, M. Lehto, IRAK-M in macrophages around septically and aseptically loosened hip implants, J. Biomed. Mater. Res. A 100 (2012) 261–268.
[28] L. Bai, R. Hang, A. Gao, X. Zhang, X. Huang, Y. Wang, B. Tang, L. Zhao, P.K. Chu, Nanostructured titanium–silver coatings with good antibacterial activity and cytocompatibility fabricated by one-step magnetron sputtering, Appl. Surf. Sci. 355 (2015) 32–44.
[29] X. Cai, M. Lin, S. Tan, W. Mai, Y. Zhang, Z. Liang, Z. Lin, X. Zhang, The use of polyethyleneimine-modified reduced graphene oxide as a substrate for silver nanoparticles to produce a material with lower cytotoxicity and long-term antibacterial activity, Carbon 50 (2012) 3407–3415.
[30] X. Hao, S. Chen, H. Yu, D. Liu, W. Sun, Metal ion-coordinated carboxymethylated chitosan grafted carbon nanotubes with enhanced antibacterial properties, RSC Adv. 6 (2016) 39–43.
[31] N. Gao, Y. Chen, J. Jiang, Ag@ Fe_2O_3-GO nanocomposites prepared by a phase transfer method with long-term antibacterial property, ACS Appl. Mater. Interfaces 5 (2013) 11307–11314.
[32] N. Wang, H. Li, W. Lü, J. Li, J. Wang, Z. Zhang, Y. Liu, Effects of TiO_2 nanotubes with different diameters on gene expression and osseointegration of implants in minipigs, Biomaterials 32 (2011) 6900–6911.
[33] J. Zhou, B. Li, S. Lu, L. Zhang, Y. Han, Regulation of osteoblast proliferation and differentiation by interrod spacing of Sr-HA nanorods on microporous titania coatings, ACS Appl. Mater. Interfaces 5 (2013) 5358–5365.
[34] J.K. Park, Y.J. Kim, J. Yeom, J.H. Jeon, G.C. Yi, J.H. Je, S.K. Hahn, The topographic effect of zinc oxide nanoflowers on osteoblast growth and osseointegration, Adv. Mater. 22 (2010) 4857–4861.

[35] J. Sun, Y. Ding, N.J. Lin, J. Zhou, H. Ro, C.L. Soles, M.T. Cicerone, S. Lin-Gibson, Exploring cellular contact guidance using gradient nanogratings, Biomacromolecules 11 (2010) 3067–3072.
[36] C. Covarrubias, M. Mattmann, A. Von Marttens, P. Caviedes, C. Arriagada, F. Valenzuela, J.P. Rodríguez, C. Corral, Osseointegration properties of titanium dental implants modified with a nanostructured coating based on ordered porous silica and bioactive glass nanoparticles, Appl. Surf. Sci. 363 (2016) 286–295.
[37] J.M. Anderson, Biological responses to materials, Annu. Rev. Mater. Res. 31 (2001) 81–110.
[38] W.F. Liu, M. Ma, K.M. Bratlie, T.T. Dang, R. Langer, D.G. Anderson, Real-time *in vivo* detection of biomaterial-induced reactive oxygen species, Biomaterials 32 (2011) 1796–1801.
[39] A. Agarwal, T.L. Weis, M.J. Schurr, N.G. Faith, C.J. Czuprynski, J.F. McAnulty, C.J. Murphy, N.L. Abbott, Surfaces modified with nanometer-thick silver-impregnated polymeric films that kill bacteria but support growth of mammalian cells, Biomaterials 31 (2010) 680–690.
[40] G.D. Shockman, J. Barren, Structure, function, and assembly of cell walls of gram-positive bacteria, Annu. Rev. Microbiol. 37 (1983) 501–527.
[41] S. Datta, N. Costantino, X. Zhou, Identification and analysis of recombineering functions from Gram-negative and Gram-positive bacteria and their phages, Proc. Natl. Acad. Sci. U. S. A. 105 (2008) 1626–1631.
[42] G. Genove, U. DeMarco, H. Xu, W.F. Goins, E.T. Ahrens, A new transgene reporter for in vivo magnetic resonance imaging, Nat. Med. 11 (2005) 450–454.
[43] A. Sengupta, U.F. Lichti, B.A. Carlson, A.O. Ryscavage, V.N. Gladyshev, S.H. Yuspa, D.L. Hatfield, Selenoproteins are essential for proper keratinocyte function and skin development, PLoS ONE 5 (2010) e12249.
[44] O. Bondarenko, A. Ivask, A. Käkinen, I. Kurvet, A. Kahru, Particle-cell contact enhances antibacterial activity of silver nanoparticles, PLoS ONE 8 (2013) e64060.
[45] S. Agnihotri, S. Mukherji, S. Mukherji, Size-controlled silver nanoparticles synthesized over the range 5–100 nm using the same protocol and their antibacterial efficacy, RSC Adv. 4 (2014) 3974–3983.
[46] J.E. Park, I.-S. Park, M.P. Neupane, T.-S. Bae, M.-H. Lee, Effects of a carbon nanotube-collagen coating on a titanium surface on osteoblast growth, Appl. Surf. Sci. 292 (2014) 828–836.
[47] G. Fu, P.S. Vary, C.-T. Lin, Anatase TiO_2 nanocomposites for antimicrobial coatings, J. Phys. Chem. B 109 (2005) 8889–8898.
[48] O. Carp, C.L. Huisman, A. Reller, Photoinduced reactivity of titanium dioxide, Prog. Solid State Chem. 32 (2004) 33–177.
[49] H.K. No, S.H. Kim, S.H. Lee, N.Y. Park, W. Prinyawiwatkul, Stability and antibacterial activity of chitosan solutions affected by storage temperature and time, Carbohydr. Polym. 65 (2006) 174–178.
[50] H. Cao, Y. Qiao, X. Liu, T. Lu, T. Cui, F. Meng, P.K. Chu, Electron storage mediated dark antibacterial action of bound silver nanoparticles: smaller is not always better, Acta Biomater. 9 (2013) 5100–5110.
[51] Y. Yuan, C. Liu, J. Qian, J. Wang, Y. Zhang, Size-mediated cytotoxicity and apoptosis of hydroxyapatite nanoparticles in human hepatoma HepG2 cells, Biomaterials 31 (2010) 730–740.
[52] G. Villatte, C. Massard, S. Descamps, Y. Sibaud, C. Forestier, K.-O. Awitor, Photoactive TiO_2 antibacterial coating on surgical external fixation pins for clinical application, Int. J. Nanomed. 10 (2015) 3367–3375.
[53] S. Mei, H. Wang, W. Wang, L. Tong, H. Pan, C. Ruan, Q. Ma, M. Liu, H. Yang, L. Zhang, Antibacterial effects and biocompatibility of titanium surfaces with graded silver incorporation in titania nanotubes, Biomaterials 35 (2014) 4255–4265.
[54] H.-L. Su, C.-C. Chou, D.-J. Hung, S.-H. Lin, I.-C. Pao, J.-H. Lin, F.-L. Huang, R.-X. Dong, J.-J. Lin, The disruption of bacterial membrane integrity through ROS generation induced by nanohybrids of silver and clay, Biomaterials 30 (2009) 5979–5987.
[55] J.J. Foti, B. Devadoss, J.A. Winkler, J.J. Collins, G.C. Walker, Oxidation of the guanine nucleotide pool underlies cell death by bactericidal antibiotics, Science 336 (2012) 315–319.
[56] Y. Liu, J.A. Imlay, Cell death from antibiotics without the involvement of reactive oxygen species, Science 339 (2013) 1210–1213.
[57] D.J. Dwyer, P.A. Belenky, J.H. Yang, I.C. MacDonald, J.D. Martell, N. Takahashi, C.T. Chan, M.A. Lobritz, D. Braff, E.G. Schwarz, Antibiotics induce redox-related physiological alterations as part of their lethality, Proc. Natl. Acad. Sci. U. S. A. 111 (2014) 2100–2109.
[58] J.A. Imlay, The molecular mechanisms and physiological consequences of oxidative stress: lessons from a model bacterium, Nat. Rev. Microbiol. 11 (2013) 443–454.
[59] M.A. Kohanski, D.J. Dwyer, B. Hayete, C.A. Lawrence, J.J. Collins, A common mechanism of cellular death induced by bactericidal antibiotics, Cell 130 (2007) 797–810.
[60] V. Etacheri, G. Michlits, M.K. Seery, S.J. Hinder, S.C. Pillai, A highly efficient $TiO_{2-x}C_x$ nano-heterojunction photocatalyst for visible light induced antibacterial applications, ACS Appl. Mater. Interfaces 5 (2013) 1663–1672.
[61] L. Dykman, N. Khlebtsov, Gold nanoparticles in biomedical applications: recent advances and perspectives, Chem. Soc. Rev. 41 (2012) 2256–2282.
[62] E. Darabpour, N. Kashef, S.M. Amini, S. Kharrazi, G.E. Djavid, Fast and effective photodynamic inactivation of 4-day-old biofilm of methicillin-resistant *Staphylococcus aureus* using methylene blue-conjugated gold nanoparticles, J. Drug Deliv. Sci. Technol. 37 (2017) 134–140.
[63] M.J. Hajipour, K.M. Fromm, A.A. Ashkarran, D.J. de Aberasturi, I.R. de Larramendi, T. Rojo, V. Serpooshan, W.J. Parak, M. Mahmoudi, Antibacterial properties of nanoparticles, Trends Biotechnol. 30 (2012) 499–511.
[64] I. Alesutan, J. Seifert, T. Pakladok, J. Rheinlaender, A. Lebedeva, S.T. Towhid, C. Stournaras, J. Voelkl, T.E. Schaeffer, F. Lang, Chorein sensitivity of actin polymerization, cell shape and mechanical stiffness of vascular endothelial cells, Cell. Physiol. Biochem. 32 (2013) 728–742.
[65] D.G. Olmedo, D. Tasat, M.B. Guglielmotti, R.L. Cabrini, Titanium transport through the blood stream. An experimental study on rats, J. Mater. Sci. Mater. Med. 14 (2003) 1099–1103.
[66] V. Antoci, C.S. Adams, J. Parvizi, H.M. Davidson, R.J. Composto, T.A. Freeman, E. Wickstrom, P. Ducheyne, D. Jungkind, I.M. Shapiro, The inhibition of *Staphylococcus epidermidis* biofilm formation by vancomycin-modified titanium alloy and implications for the treatment of periprosthetic infection, Biomaterials 29 (2008) 4684–4690.
[67] F. Costa, I.F. Carvalho, R.C. Montelaro, P. Gomes, M.C.L. Martins, Covalent immobilization of antimicrobial peptides (AMPs) onto biomaterial surfaces, Acta Biomater. 7 (2011) 1431–1440.
[68] G. Applerot, A. Lipovsky, R. Dror, N. Perkas, Y. Nitzan, R. Lubart, A. Gedanken, Enhanced antibacterial activity of nanocrystalline ZnO due to increased ROS-mediated cell injury, Adv. Funct. Mater. 19 (2009) 842–852.
[69] M.P. Brynildsen, J.A. Winkler, C.S. Spina, I.C. MacDonald, J.J. Collins, Potentiating antibacterial activity by predictably enhancing endogenous microbial ROS production, Nat. Biotechnol. 31 (2013) 160–165.
[70] P.T. Schumacker, Reactive oxygen species in cancer cells: live by the sword, die by the sword, Cancer Cell 10 (2006) 175–176.
[71] E. Palin, H. Liu, T.J. Webster, Mimicking the nanofeatures of bone increases bone-forming cell adhesion and proliferation, Nanotechnology 16 (2005) 1828–1835.
[72] Y. Zhao, M.I. Jamesh, W.K. Li, G. Wu, C. Wang, Y. Zheng, K.W. Yeung, P.K. Chu, Enhanced antimicrobial properties, cytocompatibility, and corrosion resistance of plasma-modified biodegradable magnesium alloys, Acta Biomater. 10 (2014) 544–556.